

Predicting meltponds on MOSAiC leg4 icefloe from topography using hydrological models

Torbjørn Kagel¹

¹University of Hamburg, Hamburg, Germany

Correspondence: Torbjørn Kagel (torbjorn.kagel@studium.uni-hamburg.de)

Abstract. TEXT

This work was performed within my two month internship at Alfred-Wegener-Institut (Bremerhaven) during semester break between 4th and 5th semester of B.Sc Ozeanographie (Oceanography).

Copyright statement. TEXT

5 1 Introduction

The aim of this study is to establish simple topography dependent predictions of melt pond coverage on arctic ice floes. This was done exemplarily on data from the ice floe of leg4 from MOSAiC expedition (2019/2020). The DEMs in usage were calculated from airborne photogrammetric data and later confirmed using ALS (altitude laser scanner) DEMs. The prediction was performed using two different approaches. First we used static depression filling methods and second we used a dynamical
10 flooding simulation tool to simulate snow melting onto the topography.

2 Data

Regarding data coverage, there are three pre-melting orthophotographs within the period of March to May of 2020 that are usable, compare figure 1. Since photogrammetric data is dependent on weather and light conditions (polar night lasts until
15), the data choice is shrunked to these three dates. These photos serve as our main source of information in this work. DEM data calculations then comes from *cite: niklas-paper*.

ALS data as an active recording method however is not dependent to these limiting circumstances, thus giving us more choices to analyse for example how well predictions are possible from mid-winter recordings (January), compare figure 2.

Melting starts shortly after 25.05 and continues until 26.07 with a maximum pond coverage of 22% (Webster et al., 2022).

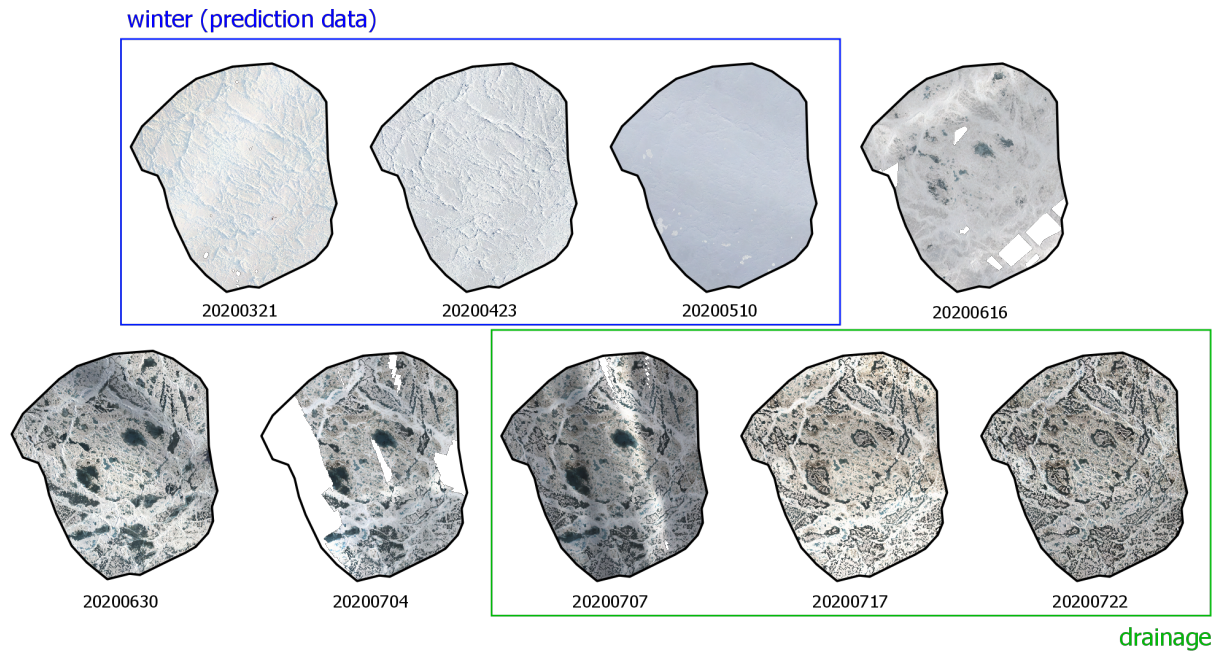


Figure 1. Overview of available orthophotos of leg4 ice floe. 21.03, 24.03 and 10.05 are used to generate predictions, 16.06, 30.06, 07.07, 17.07 and 22.07 are used as references. Drainage of melt ponds is observed beginning on 07.07. The recording of 04.07 will not be used because of low coverage.

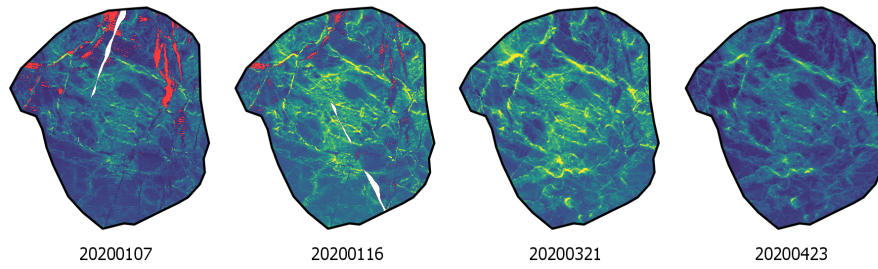


Figure 2. Overview of selected ALS DEMs of leg4 ice floe. Red areas are rough sketches of open water to visualise the formation of the ice floe. 07.01 and 17.01 are chosen to see how topographical prediction performs with older data. 21.03 and 24.03 are used to compare predictions to the photogrammetric recordings. When speaking of drainage, we refer to intra-drainage (drainage inside of the melt pond area).

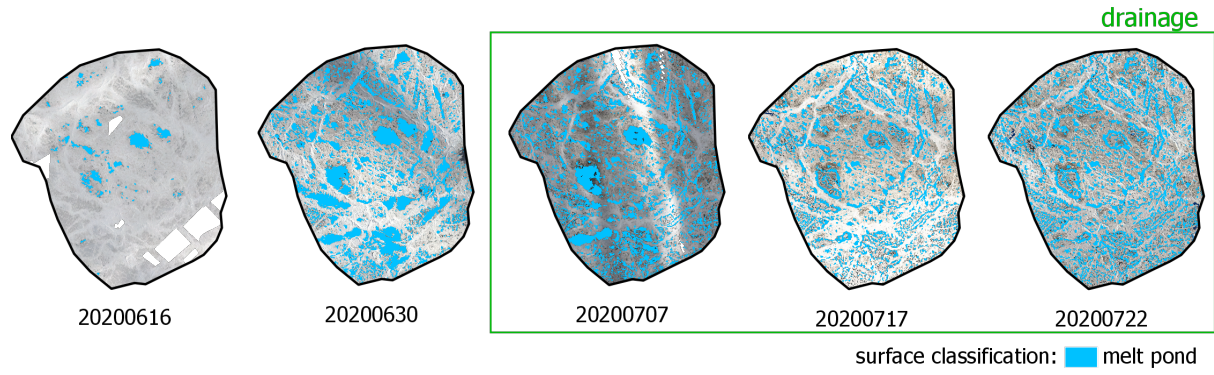


Figure 3. Classified surfaces for summer recordings. Detection is performed with *Quelle/Algo? -> Niklas*. Highest coverage is observed on 22.07 with 23% (difference to value of Webster et al. (2022) may come to different area of calculation). Highest mean size of large melt ponds (area > 100m²) however is observed on 30.06 with 777m² (07.07: 527m² and 22.07: 536m²), confirming drainage starting on 07.07 in our dataset.

3 Methods

20 **3.1 Statistical Classification**

To quantify the obtained results we compared the location and size of predicted melt ponds to the actual, observed melt ponds from summer. This also allows comparison of the static to the dynamic models. To visualise the results three different plots are established. Besides that we concern the statistical classification measurements of precision, recall and F-score. F-score as a combination of both precision and recall will serve as our main assessment measure for comparing performances of different
25 dates and tools.

-> plots (accuracy map, accuracy table, confusion matrix) vorstellen

3.2 Static models

The static approach is based on depression filling algorithms. There a lot of implementations of this method in different GIS
30 softwares or libraries. We used three different tools to compare and discuss. They all come from different backgrounds and are open-source which makes the comparison interesting. The used tools are the following:

1. Pysheds (Bartos, 2020)
2. RichDEM (Barnes, 2013)
3. whiteboxtools (Lindsay, 2017)

35 **3.2.1 Algorithms**

-> explain different algorithms

3.2.2 Application

-> depth calculation (UML einfügen?)

40

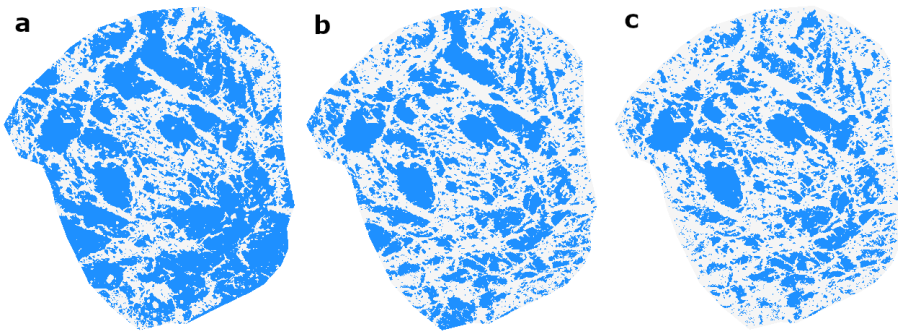


Figure 4. Pond prediction from the used tools for 21.03. **a:** pysheds, **b:** RichDEM, **c:** whiteboxtool. The predicted coverage is highest with pysheds (60%), and least with whiteboxtool (38%). Using RichDEM we predict a coverage of 44%.

3.3 Dynamic Models

The dynamic approach is more complex. For this work the flood simulation tool Itzi (Courty et al., 2017) was used. Itzi is used for rapid precipitation events and in its most basic application takes an DEM as input and calculates water depths, velocities and directions from given precipitations amount per time. Obviously it is therefore not meant as a melting simulation tool.

45 However with a few adaptations a useful prediction can be performed (see section 3.3.2).

3.3.1 Algorithm

-> basic algorithm explanation (citing the paper)

3.3.2 Itzi adaptation and procedure

For using Itzi as an melting simulation rather than a flood simulation tool, a few adaptations have to be performed beforehand:

- 50 1. The computational period of 36 days (25.05 - 30.06) is scaled down to 36 hours. This was done because Itzi has a fixed time step of 1 second. Putting in a simulation duration of 36 days results in very high computation times.

2. The Input DEM was resampled to 5m resolution. This has the same benefit of lowering computation time, but also reducing noise in the input data. Later the original resolution of 0.5m was also tested.

3. Since Itzi simulates precipitation we need some sort of water equivalent from the available snow. For testing we used spatial and temporal constant melting with fixed values between 1 and 10mm/h (in computational scale). For a more realistic and applicable approach we calculated SWE (snow water equivalents) from recorded snow depths. This was done by methods described by Wagner et al. (2022) and with data from Itkin et al. (2022) (compare figure ??)

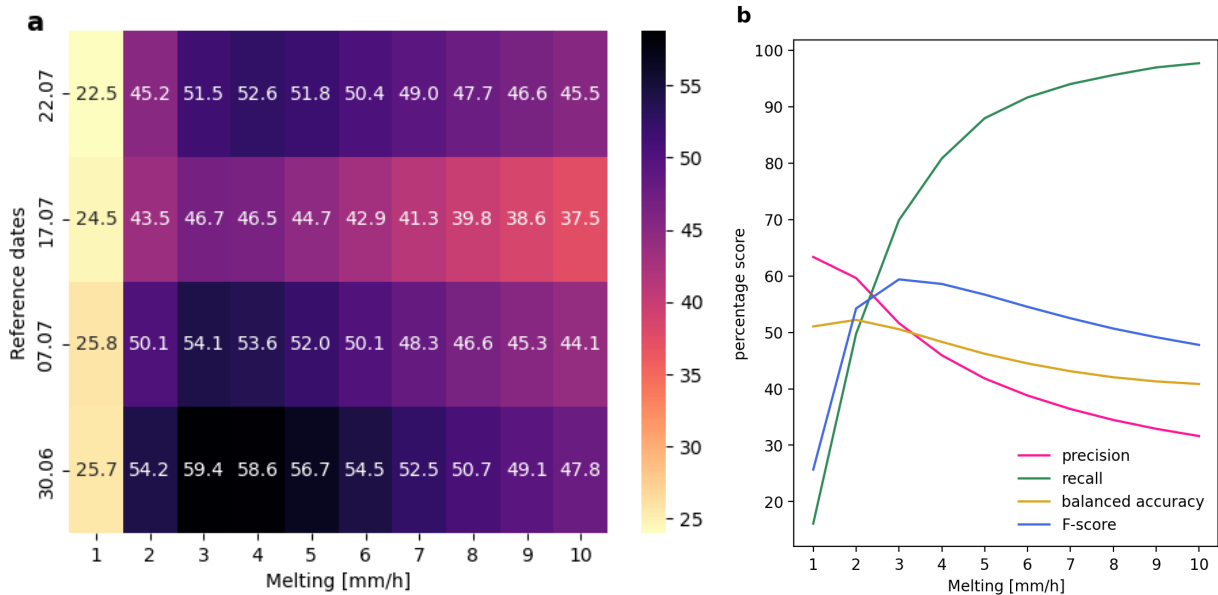


Figure 5. a: F-score confusion matrix for different melting rates performed on the DEM from 23.04 against the reference dates, best performance is achieved with a melting rate of 3mm/h compared to 30.06. **b:** Overview of precision, recall, (balanced) accuracy and F-Score of the different melting rates. Reference date is 30.06. Recalls rises with rising predicted pond coverage, while precision sinks.

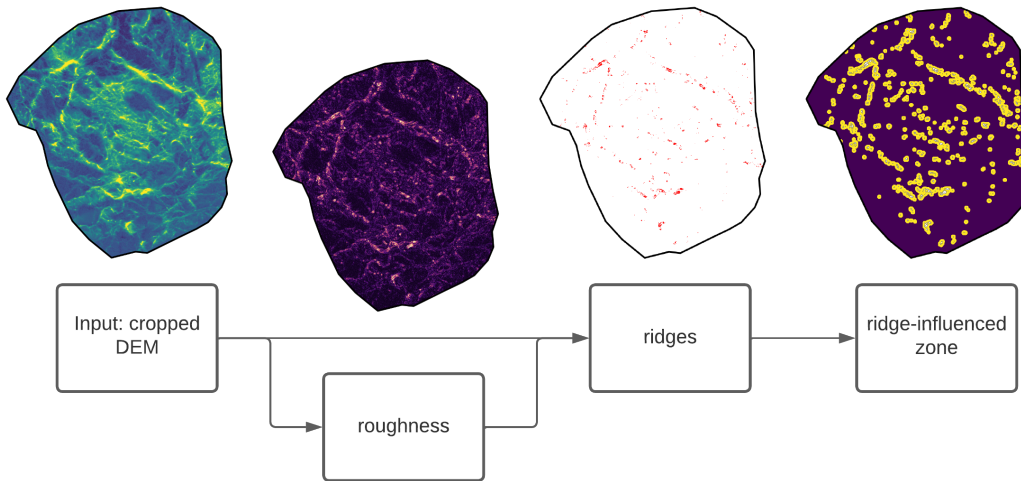


Figure 6. Procedure for calculating a melting distribution only from an input DEM and snow depth data. Roughness is classified according to GDALs algorithm, whereas ridges are classified by height in DEM > 1.5m and roughness R > 0.3. Ridge influenced zones (RIZ) are areas within a radius of 10 meters of ridges.

We assigned a melting rate of 6.9mm/h to RIZ and 2.7mm/h to the rest of the level area on the ice floe. These rates are calculated from measured snow depths from Itkin et al. (2022). They did a classification to three roughness categories: (1) level, (2) rubble and (3) ridges. Measured snow depths are then assigned to each of these classes (ridges: 0.30m and level: 0.15m). The classification shown in figure 6 results in area coverage of ridges similar to observed values from Itkin et al. (2022). From these snow depth we calculated SWE (Wagner et al., 2022) and scaled the melting rate according to the temporal information.

A categorization to first-year-, second-year- or multi-year-ice (FYI, SYI, MYI) is not practical. While there is a difference in winter and early spring concerning snow depths, when melting starts, snow is evenly distributed across different ice age types (Itkin et al., 2022). Also we did not perform a classification for rubble. Our procedure is adapted from transect data and the goal is to keep it as general as possible, which is why we only used the most diverse classes with very different snow depths.

4 Results

4.1 Static models

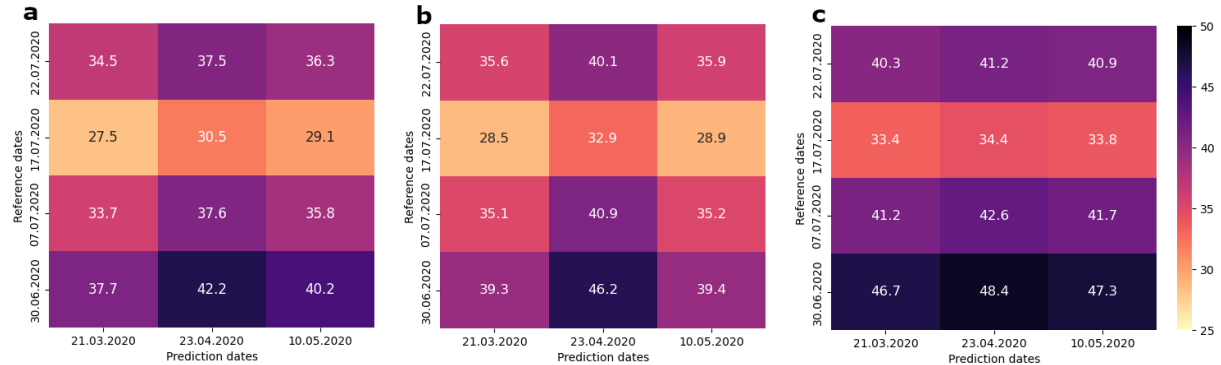


Figure 7. Precision matrix, **a:** pysheds (avg. score: 35.2%), **b:** RichDEM (avg. score: 36.5%), **c:** whiteboxtool (avg. score: 41.0%)

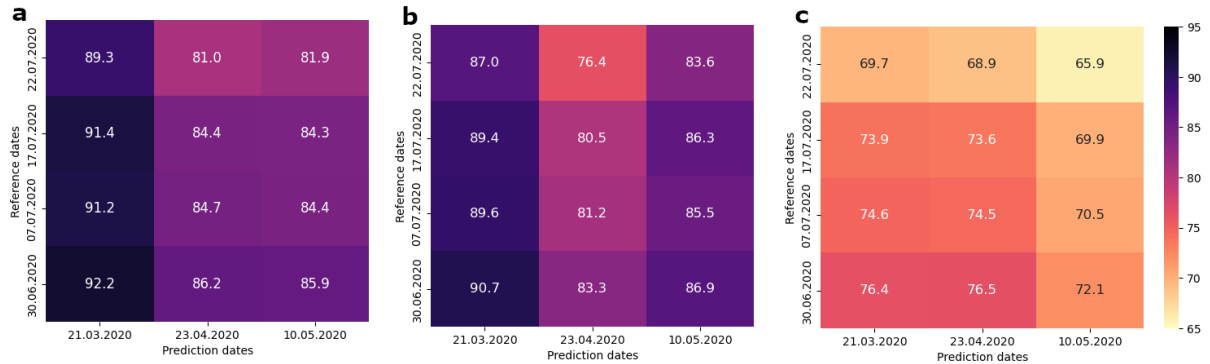


Figure 8. Recall matrix, **a:** pysheds (avg. score: 86.4%), **b:** RichDEM (avg. score: 85.0%), **c:** whiteboxtool (avg. score: 72.2%)

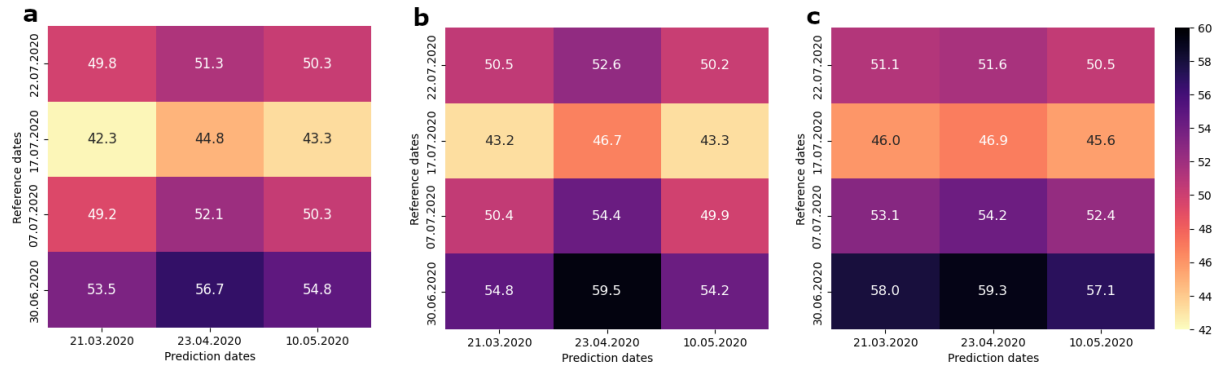


Figure 9. F-score matrix, **a:** pysheds (avg. score: 49.8%), **b:** RichDEM (avg. score: 50.8%), **c:** whiteboxtool (avg. score: 52.1%)

70 Figures 7, 8 and 9 compare the different tools with all photogrammetric data available. Concerning precision whitebox tool scores the highest average across all dates, and also the highest single score (23.04 vs. 30.6 - 48.4%) is achieved with whiteboxtools algorithm. Recall is highest with pysheds, which is because pysheds overestimates pond coverage drastically (compare fig. 4).
 75 Regarding F-score whiteboxtool has the highest average performance, while RichDEM has the highest single score (23.04 vs. 30.06 - 59.5%). Generally we can observe that 24.03 as prediction date and 30.06 as reference date scores the best results. With 21.03 and 10.05 scores being circa equally distant to 24.03. With later reference dates performance of static models shrinks, which is because of unpredictable drainage (compare section 4.4).

Taking a closer look at the spatial distribution of resulting confusion value, we can observe several aspects where the static models perform well and where they struggle.

80 First of the prediction of large melt ponds is generally good. The largest central, coherent ponds with areas above 2000m² are all predicted with just minor edge discrepancies.

However there certain areas on the floe that do not perform well. We will discuss these further in section 4.4

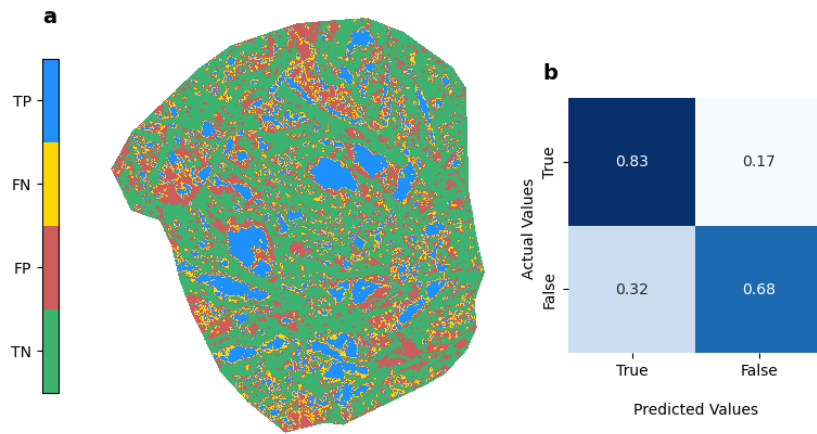


Figure 10. RichDEM confusion plots for the best performing combination (compare figure 9b). **a:** confusion map, blue: true positive, green: true negative, yellow: false negative, red: false positive. **b:** confusion matrix, normalised for actual values (reference dates)

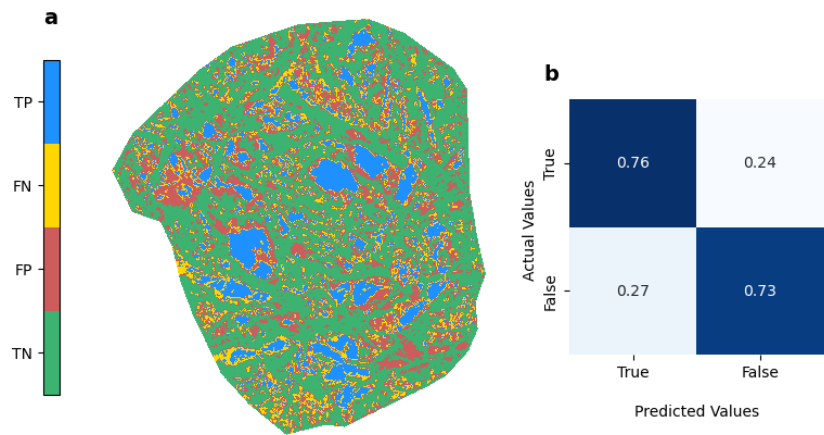


Figure 11. Whiteboxtool confusion plots for the best performing combination (compare figure 9c). **a:** confusion map, blue: true positive, green: true negative, yellow: false negative, red: false positive. **b:** confusion matrix, normalised for actual values (reference dates)

4.2 Dynamic model

-> Ergebnis depths von itzi einfügen (wie bei statisch)

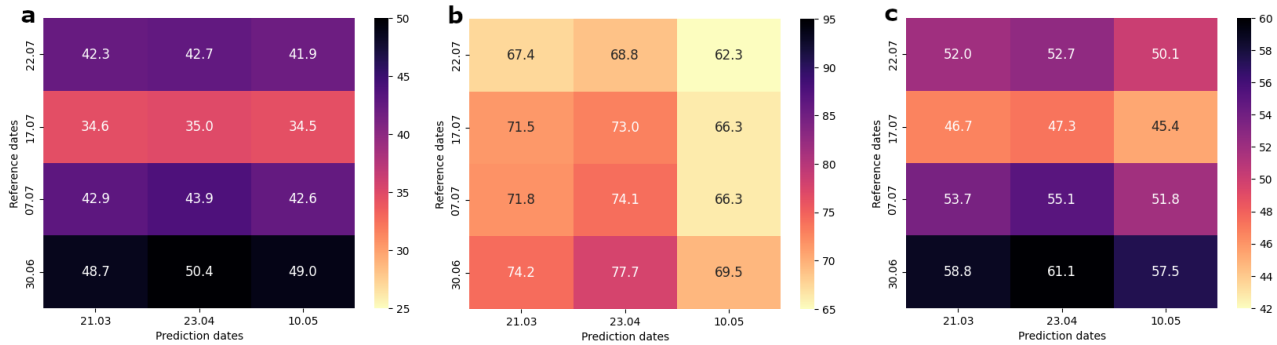


Figure 12. Resulting comparison matrices from Itzi with melting distributed according to 6. **a:** precision, **b:** recall, **c:** Fscore

85 Compared to spatial constant melting (figure 5) we could improve Fscore by about 2%.

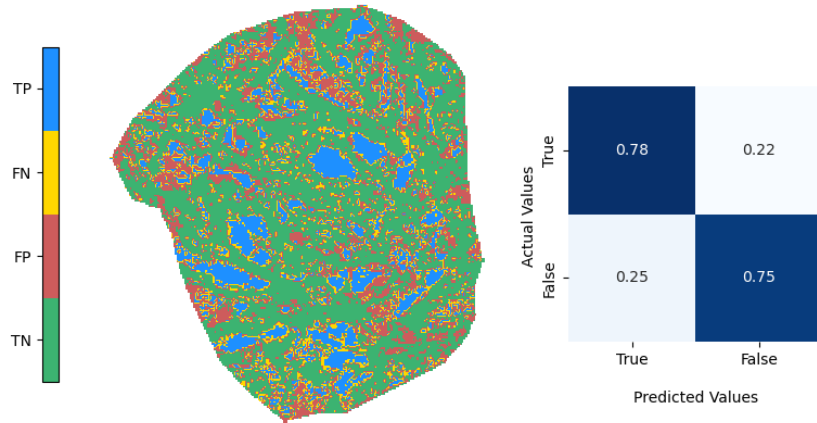


Figure 13. Itzi confusion plots for the best performing combination (compare figure 12c). **a:** confusion map, blue: true positive, green: true negative, yellow: false negative, red: false positive. **b:** confusion matrix, normalised for actual values (reference dates)

4.3 Interim time step - 16.06

There is only one interim time step, where melt ponds are not yet completely formed. The recording is from 16.06 and shows some interesting features, compare figure 3. We can see that melting does not occur spatially equally distributed but rather starts on specific locations. The large, central melt pond occurs first along with some others. Of course they are not yet fully developed in size. Modelling this temporal non-uniform evolution is not performed in this work. It might also be rather difficult when only taking topographical features into account.
90

4.4 Quantifying drainage

The main problem occurring when predicting melt ponds from topographical features is the difficulty of large drainage channel networks which form during melting (compare fig. 14). These are obviously not predictable from surface topography and
95 would require a much more complex system of modelling to be taken into account.

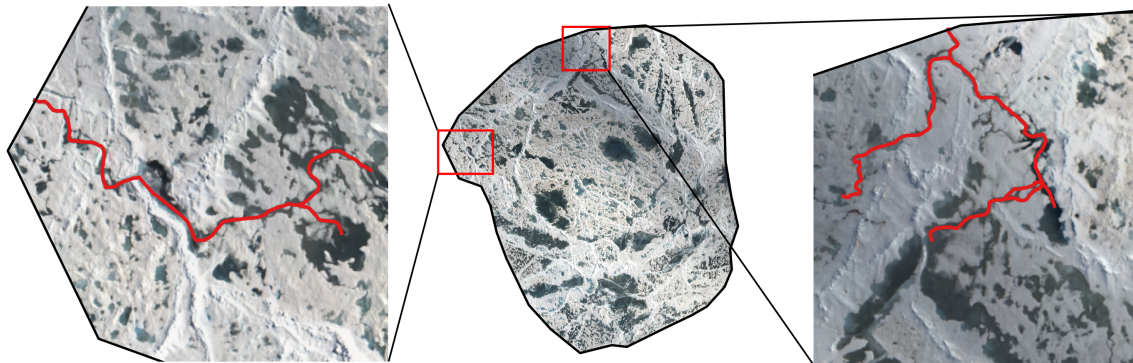


Figure 14. Observable drainage channels on 30.06.

4.5 Comparing to ALS DEMs

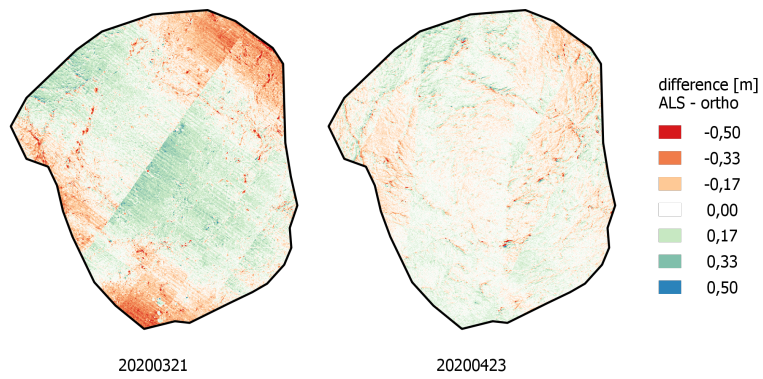


Figure 15. Difference of ALS and photogrammetric data. On 21.03 we can observe the swath width of the laser scanner, while on 24.03 there seem to be some general differences of both methods.

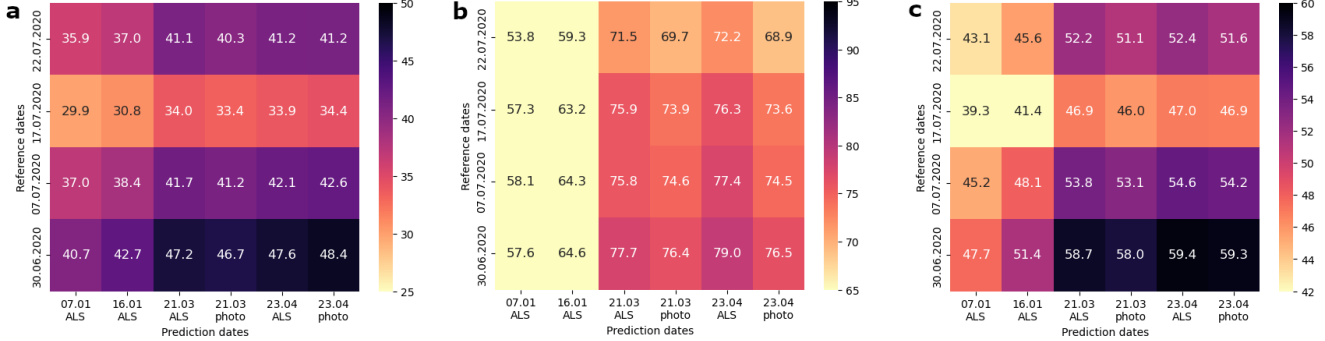


Figure 16. Comparison of ALS to photogrammetric data with static model whiteboxtool. **a:** precision, **b:** recall, **c:** Fscore. We can observe a slight improvement with ALS data regarding F-score of 0.7% on both 21.03 and 23.04. The first two columns are the winter dates 07.01 and 16.01 where only ALS recordings are available. As expected performance gets worse when looking at earlier data.

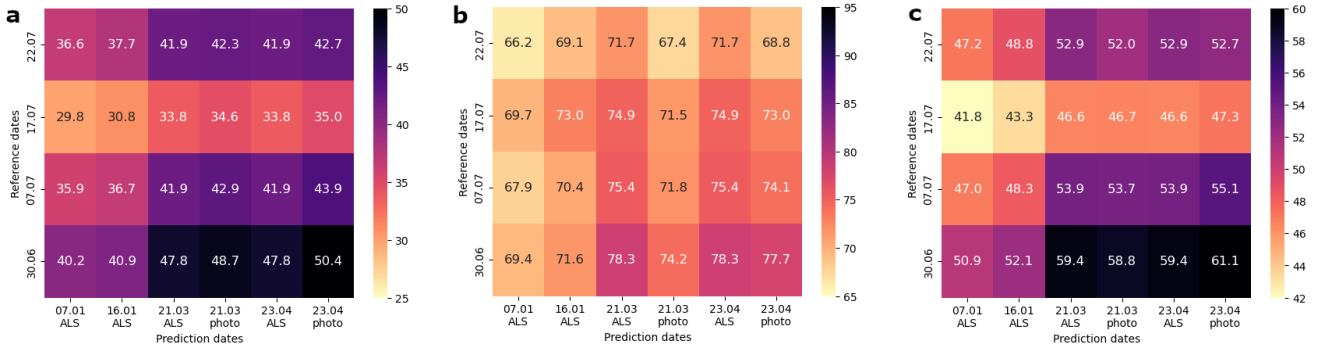


Figure 17. Comparison of ALS to photogrammetric data with dynamic model itzi. **a:** precision, **b:** recall, **c:** Fscore.

5 Discussion

-> Schwierigkeiten, da DEM sich selbst abträgt

-> drainage channels (figure: ausschnitt aus photo) nicht topographisch vorhersagbar

100 6 Conclusions

TEXT

Code availability. TEXT

Data availability. TEXT

Code and data availability. TEXT

105 *Sample availability.* TEXT

Video supplement. TEXT

Appendix A

A1

Author contributions. TEXT

110 *Competing interests.* TEXT

Disclaimer. TEXT

Acknowledgements. TEXT

References

- Barnes, R.: Priority-flood: An optimal depression-filling and watershed-labeling algorithm for digital elevation models,
115 https://doi.org/10.1016/j.cageo.2013.04.024, 2013.
- Bartos, M.: pysheds: simple and fast watershed delineation in python, https://doi.org/10.5281/zenodo.3822494, 2020.
- Courty, L. G., Pedrozo-Acuña, A., and Bates, P. D.: Itzi (version 17.1): an open-source, distributed GIS model for dynamic flood simulation,
Geoscientific Model Development, 10, 1835–1847, https://doi.org/10.5194/gmd-10-1835-2017, 2017.
- Itkin, P., Hendricks, S., Webster, M., von Albedyll, L., Arndt, S., Divine, D., Jaggi, M., Oggier, M., Raphael, I., Ricker, R., Rohde, J.,
120 Schneebeli, M., and Liston, G.: Sea ice and snow characteristics from year-long transects at the MOSAiC Central Observatory, 2022.
- Lindsay, J.: Whiteboxtool, https://github.com/jblindsay/whitebox-tools, 2017.
- Wagner, D. N., Shupe, M. D., Cox, C., Persson, O. G., Uttal, T., Frey, M. M., Kirchgaessner, A., Schneebeli, M., Jaggi, M., Macfarlane, A. R.,
Itkin, P., Arndt, S., Hendricks, S., Krampe, D., Nicolaus, M., Ricker, R., Regnery, J., Kolabutin, N., Shimanshuck, E., Oggier, M., Raphael,
I., Stroeve, J., and Lehning, M.: Snowfall and snow accumulation during the MOSAiC winter and spring seasons, The Cryosphere, 16,
125 2373–2402, https://doi.org/10.5194/tc-16-2373-2022, 2022.
- Webster, M. A., Holland, M., Wright, N. C., Hendricks, S., Hutter, N., Itkin, P., Light, B., Linhardt, F., Perovich, D. K., Raphael, I. A., Smith,
M. M., von Albedyll, L., and Zhang, J.: Spatiotemporal evolution of melt ponds on Arctic sea ice: MOSAiC observations and model
results, Elementa: Science of the Anthropocene, 10, https://doi.org/10.1525/elementa.2021.000072, 2022.